

Small BODIPY Probes for Combined Dual ^{19}F MRI and Fluorescence Imaging

Anh Minh Huynh,^[a] Andreas Müller,^[b] Sonja M. Kessler,^[c] Sarah Henrikus,^[a] Caroline Hoffmann,^[a] Alexandra K. Kiemer,^[c] Arno Bücken,^[b] and Gregor Jung^{*[a]}

The combination of the two complementary imaging modalities ^{19}F magnetic resonance imaging (MRI) and fluorescence imaging (FLI) possesses high potential for biological and medical applications. Herein we report the first design, synthesis, dual detection validation, and cytotoxic testing of four promising BODIPY dyes for dual ^{19}F MRI–fluorescence detection. Using straightforward Steglich reactions, small fluorinated alcohols were easily covalently tethered to a BODIPY dye in high yields, leaving its fluorescence properties unaffected. The synthesized compounds were analyzed with various techniques to demonstrate their potential utility in dual imaging. As expected,

the chemically and magnetically equivalent trifluoromethyl groups of the agents exhibited a single NMR signal. The determined longitudinal relaxation times T_1 and the transverse relaxation times T_2 , both in the lower second range, enabled the imaging of four compounds in vitro. The most auspicious dual ^{19}F MRI–fluorescence agent was also successfully imaged in a mouse post-mortem within a 9.4 T small-animal tomograph. Toxicological assays with human cells (primary HUVEC and HepG2 cell line) also indicated the possibility for animal testing.

Introduction

Today, imaging techniques are indispensable tools in any kind of life science. Each method has its unique strengths and weaknesses with varying spatial and temporal resolution limits, so that a single imaging modality can be used with great advantage for one application, but is poorly suited for other applications. For this reason, no imaging technique can provide all information of the object of interest; therefore, dual imaging is highly desired. Dual imaging is defined by the synergistic combination of two orthogonal imaging modalities which allows combination of the inherent advantages of each imaging technique. Well-known examples include various combinations between positron emission tomography (PET), single photoemission computed tomography (SPECT), fluorescence imaging (FLI), ultrasound imaging, and magnetic resonance imaging (MRI).^[1] One of the most used combinations is dual MRI and FLI.^[2] MRI has high spatial and temporal resolution relative to other noninvasive imaging modalities as well as deep tissue penetration, but lacks sensitivity and specificity. In contrast, FLI is often used for molecular imaging, for example, in

histology, due to its high sensitivity and specificity for target detection. The disadvantage of FLI is that quantification is challenging. Moreover, detrimental light scattering and absorption restrict its application to low tissue depth.

MRI, as one of the most important noninvasive methods, is usually based on the H_2O proton relaxation times, which may vary among different tissues and which can be locally accelerated in the presence of contrast agents. These are often paramagnetic metal ion complexes with the most prominent metal being gadolinium (Gd^{3+}). In 2006, however, a possible link between Gd-containing contrast agents and a medical condition called nephrogenic systemic fibrosis (NSF) was found.^[3] Therefore, it is highly desirable to establish more abundant ions as alternatives, such as iron (Fe^{3+})^[4] or manganese (Mn^{2+}),^[5] which might overcome these toxic effects. Another way may be to switch the nucleus from ^1H to ^{19}F MRI. The ^{19}F nucleus is also well suited for MRI, given its natural abundance of 100%, high gyromagnetic ratio, spin of $1/2$ and high receptivity of 0.834 relative to ^1H . Additionally, there is no ^{19}F MRI background in biological systems. Hence, in the last few years numerous papers about ^{19}F MRI have been published.

Currently, most of the ^{19}F MRI agents or tracers are perfluorocarbon emulsions (PFC), which contain a high number of covalently bound ^{19}F atoms and are easily modified for further applications.^[6] Unfortunately, PFCs have shown several disadvantages such as heterogeneity, instability, multiple ^{19}F signals, difficult synthesis, and also accumulation or even retention within organs for a couple of months.^[6c,7] These drawbacks are largely overcome in a second group of ^{19}F MRI tracers based on small molecules.^[8] The as-yet-described molecules are chemically stable, easy to synthesize, and have shown short

[a] A. M. Huynh, S. Henrikus, C. Hoffmann, G. Jung
Department of Chemistry, Biophysical Chemistry,
Saarland University, Campus, 66123 Saarbrücken (Germany)
E-mail: g.jung@mx.uni-saarland.de

[b] A. Müller, A. Bücken
Clinic of Diagnostic and Interventional Radiology,
Saarland University Medical Center, 66424 Homburg (Germany)

[c] S. M. Kessler, A. K. Kiemer
Department of Pharmacy, Pharmaceutical Biology,
Saarland University, 66123 Saarbrücken (Germany)

Supporting information for this article can be found under <http://dx.doi.org/10.1002/cmdc.201600120>.

residence times in mice.^[8a] Furthermore, as a result of the low quantity of ^{19}F nuclei relative to ubiquitous protons, these tracers possess chemically and magnetically equivalent fluorine atoms to maximize the generated magnetic resonance signal. Despite the mentioned advantages, the limitations of small-molecule tracers are their difficult modification after completed synthesis and low sensitivity. Furthermore, a relatively high probe concentration relative to PFCs is still required.

A convenient way to promote ^{19}F MRI is the combination with FLI for subsequent co-localization and validation of acquired images. Fluorescent dyes are easy to tether covalently to the MRI contrast agent. Recently, FLI was shown to serve as a powerful tool in surgery to guide the scalpel.^[9] An intriguing example is the visualization and complete removal of ovarian cancer with the help of fluorescein-labeled folate.^[10] Nevertheless, at the moment, dual ^{19}F MRI and fluorescence agents consist of nanoemulsions, nanoparticles, or amphiphiles combined with a fluorophore.^[6f,h,11] For the combination of MRI and FLI, a brief and compact fluorescent dye as good starting point for derivatization is mandatory. Among the vast number of fluorophores, the family of boron dipyrromethene dyes, also known as BODIPY dyes, possess these properties. They show narrow emission bands, high quantum yields and high photostability,^[12] are chemically stable, and can be easily modified. Accord-

ingly, BODIPY dyes are widely used as fluorescent switches, laser dyes, biomolecule markers, and chemosensors.^[13]

On account of the recent trends, herein we describe the syntheses of five dual imaging probes 1–5 for ^{19}F MRI and fluorescence imaging (Figure 1). The fluorescent part consists of the well-known tetramethyl-BODIPY scaffold (TMBDP) which has consistently shown very good fluorescence properties in past applications.^[14] BODIPY dyes have already been established as dual modality agents for ^{18}F PET and FLI.^[15] Here, the ^{19}F MRI part derives from commercially available trifluoroethyl alcohol, perfluoro-*tert*-butyl alcohol, pentafluorophenol, and two further synthesized alcohols, which contain 18 or 27 ^{19}F nuclei. Subsequently, we characterized the molecules by fluorescence spectroscopy, ^{19}F NMR spectroscopy, and relaxometry. We successfully mapped different concentrations down to the lower-millimolar range of the synthesized compounds within a 9.4 T small-animal magnetic resonance tomograph (MRT). Finally, 3-(4,5-dimethylthiazol-2-yl)-2,5-diphenyltetrazolium bromide (MTT) assays with human umbilical vein endothelial cells (HUVEC) and human liver carcinoma cells (HepG2) revealed their low toxicity, making our compounds candidates for further *in vivo* experiments.

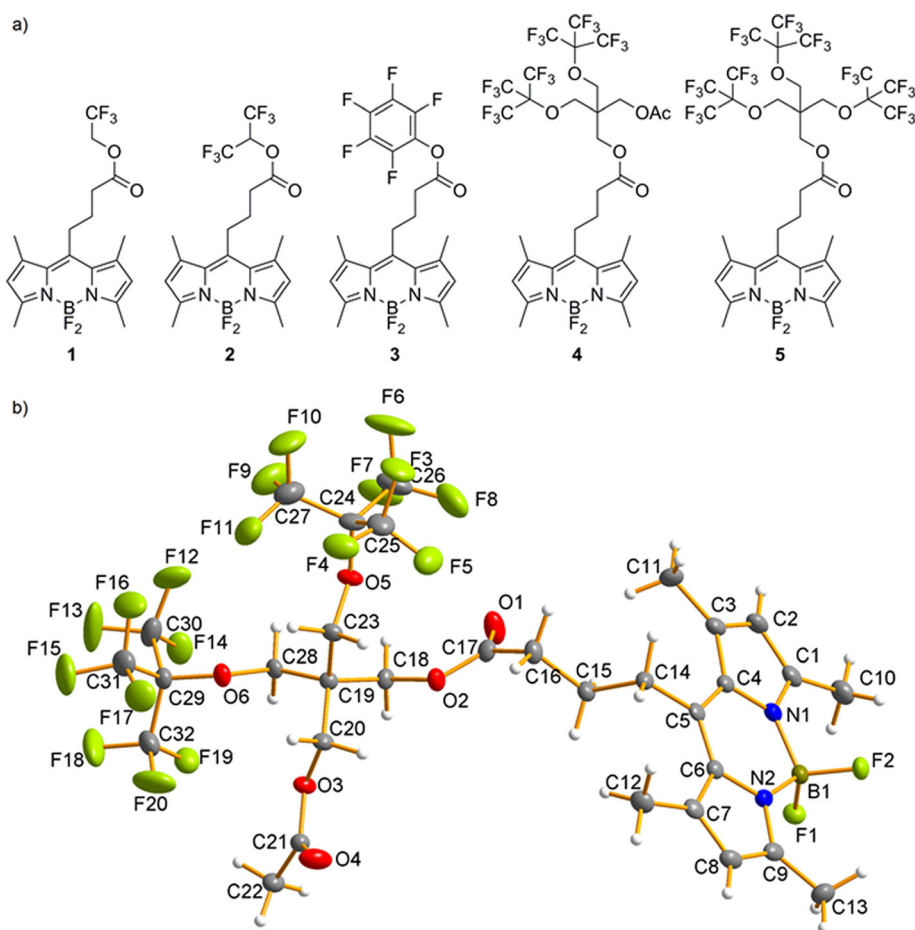


Figure 1. a) Structures of the synthesized dual imaging tracers. b) Crystallographic structure of compound 4.

Results and Discussion

The synthesis of the dual imaging contrast agents follows a simple and straightforward strategy (Table 1). In a standard Steglich reaction, the carboxylated BODIPY **6**, which was synthesized according to a published method,^[16] reacts with five different alcohols to form the corresponding esters. The alcohols **7–9** for the compounds **1–3** are commercially available.

However, the perfluorinated alcohol **10** for compound **5**, which was used in other molecules for ¹⁹F MRI, and which therefore has great potential for similar applications,^[8a,b] was synthesized as described (Scheme 1).^[17] The standard Steglich condensation between alcohol **10** and BODIPY **6** turned out to be too unreactive, likely due to the low nucleophilicity of the alcohol. The yields were increased from 20% to 99% with a reaction variation using Sc(OTf)₃, in addition to the reagents 4-(dimethylamino)pyridine (DMAP) and *N,N'*-diisopropylcarbodiimide.^[18] Interestingly, during the synthesis of alcohol **10**, a remarkable side product was collected. After isolation, NMR analysis showed that the side product to be the benzyl- and acetyl-protected pentaerythritol **11**, which can appear during the cleavage of the orthoacetate protection group (Figure 2).^[19] With this compound, we were able to synthesize the acetyl-protected alcohol **12** by following the already known synthesis pattern. The structure of the finally obtained compound **4** was confirmed by X-ray crystallography (Figure 1b).

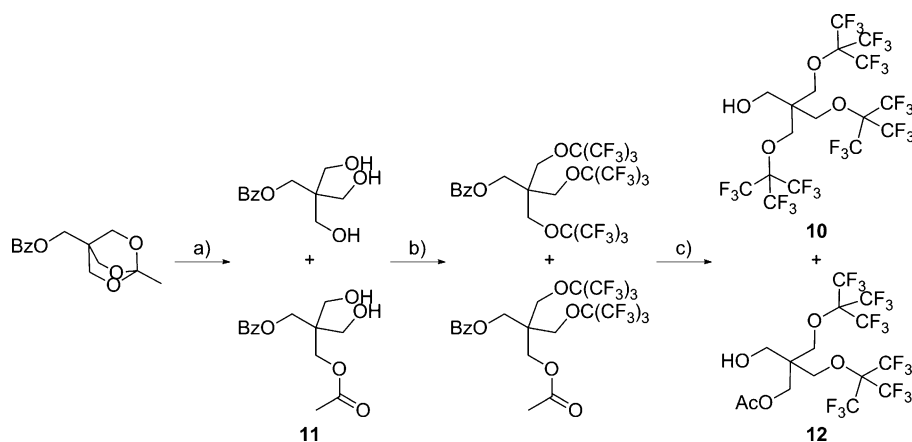
After the successful synthesis, we first validated the fluorescence properties of the compounds **1–5**. As we did not change the chromophore system, all synthesized fluorescent dyes maintained the electronic spectra of the parent compound TMBDP ($\lambda_{\text{exc}}=501$ nm, $\lambda_{\text{em}}=513$ nm; Figure 2a).^[20] We therefore assume that the synthesized BODIPY dyes have the same good optical properties as the parent BODIPY dye, verified for **4** and **5** by fluorescence microscopy with appropriate filter combinations (Figure 2b and Supporting Information Figure S47). Afterward, we measured ¹⁹F NMR spectra to verify their magnetic activity. As expected, the spectra of the four compounds **1**, **2**, **4**, and **5** showed a strong singlet from the chemically and magnetically equivalent CF₃ groups and a weak

Table 1. Synthesis of dual imaging tracers **1–5**.

Entry	Alcohol	Product	Yield [%]
1 ^[a]		1	91
2 ^[a]		2	88
3 ^[a]		3	82
4 ^[b]		4	99
5 ^[b]		5	81

[a] DMAP, DCC, CH₂Cl₂, 0 °C for 1 h, then RT, 24 h; [b] DMAP, Sc(OTf)₃, DIPC, CH₂Cl₂, -8 °C for 1 h, then RT, 2 d.

quartet signal from the BF₂ group (Figures S3, S10, S21, and S28). In contrast, the ¹⁹F NMR spectrum of compound **3** showed multiple weak signals from the different fluorine atoms next to carbon and the BF₂ unit (Figure S17). The BODIPY **3** mainly was synthesized to study the influence of various fluorine nuclei on MRI.



Scheme 1. Synthesis of alcohol **10** and **12** after reaction conditions from Jiang and Yu.^[17] Reagents and conditions: a) HCl (0.01 N), MeOH, RT, 38%; b) (CF₃)₃COH, DEAD, Ph₃P, 4 Å MS, THF, 45 °C, ~64–76%; c) AlCl₃, anisole, CH₂Cl₂, 0 °C, ~64–85%.

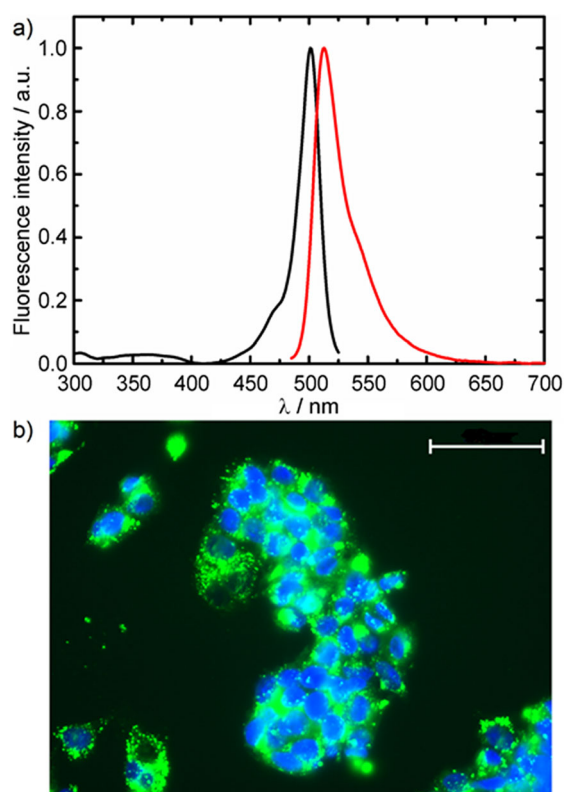


Figure 2. a) Excitation (black) and emission (red) spectra of compound **5** (CH_2Cl_2 , 100 nm). b) Fluorescence micrograph of HepG2 cells after incubation with compound **4** (50 μM , green) for 1 h and subsequent fixation. Counterstaining of nuclei was achieved with DAPI (blue). Scale bar: 50 μm .

Table 2. Estimated relaxation times for compounds 1–5.		
Compound	T_1 [s] ^[a]	T_2 [s] ^[a]
1	4.8	1.8
2	3.9	1.7
3	2.3	– ^[b]
4	2.2	1.5
5	2.1	1.3

[a] Performed in CHCl_3 at 30 °C, determined with a benchtop relaxometer ($B_0 = 1.41$ T); concentrations were in the range of 20–25 mM. [b] Could not be fitted due to multiple fluorine signals.

Because of the clear ^{19}F NMR signals, we then determined the longitudinal relaxation times T_1 and the transverse relaxation times T_2 with a 1.41 T ^{19}F NMR benchtop device. The relaxation times of the synthesized compounds 1–5 were found to be in the area of several seconds (Table 2) with a definite correlation to the size of the fluorinated alcohol. The larger the side group, the shorter the T_1 value in particular, which is in agreement with the influence of the rotational diffusion on the relaxation times. Hence, the ratio of T_1 to T_2 dropped from 2.7 to 1.5 for the most fluorinated compounds **4** and **5**. Only T_2 of **3** indicates rapid dephasing and concomitant loss of an FID signal. The decay times were higher by a factor of 10–30 in comparison with a similar ^{19}F MR reporter^[8a] in micelles, 3–8

times higher than a nanoemulsion of a small ^{19}F MR reporter^[8c] and 2–3 times higher than PFC nanoparticles.^[6g] Nevertheless, the shortest T_1 values were found for the bulky compounds **4** and **5** with 2.2 seconds, which are still short enough for promising MRI data collection.

With knowledge about the relaxation times, the next step was to detect compounds 1–5 at various concentrations in vitro inside the 9.4 T small-animal MRT. BODIPYs **1** and **2** required concentrations of ~60 to 100 mM for clear detection, which is only slightly diminished relative to the BF_2 moiety of commercial pyromethene 546 (Figures S7, S14, and S46). Compound **3** was spectroscopically silent, even at concentrations higher than 100 mM. We explain this finding by the low number of magnetically equivalent fluorine atoms and the rapid dephasing. In contrast, BODIPYs **4** and **5**, which have 18 and 27 fluorine atoms, respectively, enabled detection of concentrations at 20 and 10 mM (Figure 3a,b). These concentrations are in agreement with published detection limits in this field, which have the same or even higher number of fluorine atoms per molecule.^[8] With the image of the different concentrations of compounds **4** and **5**, it is possible to verify the linearity between signal-to-noise ratio (SNR) and concentration (Figure 3c), which was shown in previous publications.^[8a,c] Considering the voxel size of $1 \times 1 \times 5$ mm³ and the minimal detected concentration of 10 mM, the calculated minimal fluorine atom number required for our setup is 8×10^{17} fluorine atoms per voxel, which is also valid for the fluorine atoms of the BF_2 unit under altered resonance conditions (see Figure S46). A key step for further in vivo applications is visualization of the synthesized agents under a biological environment. As an initial step in this direction, we injected 100 μL of a 100 mM solution of compound **5** into the muscle of a mouse post-mortem (Figure 3d,e). We used black-light excitation for FLI, similarly to the successful approach in surgery.^[9,10] The red shift of the observed fluorescence presumably arises from reabsorption or aggregation.^[21]

For future medical or biological experiments, it is also crucial to test the cytotoxicity of the synthesized molecules. HUVEC isolated from human vessels served as a model with utmost relevance for the human in vivo situation.^[22] Human HepG2 is a model cell line frequently used for toxicity studies.^[23] Both cell types were used in a metabolic MTT assay, in which conversion of the added MTT thiazolium into blue formazan serves as readout for cell viability. The four BODIPYs **1**, **2**, **4**, and **5**, including the precursor molecule **6**, were investigated. In the case of the uptake of the synthesized agents and the cleavage of the ester functionality, it is important to know if the decomposition product **6** is toxic. Still, the free carboxyl group most likely inhibits cellular uptake, which is why we used the ethanol ester **13** as a reference compound. The resulting IC_{50} values in HepG2 for BODIPY **6** and **13** show that these compounds are probably toxic for these cells (Table 3). Most interestingly, in case of the HepG2 cells, the synthesized BODIPYs **1**, **2**, **4**, and **5** were found to be less toxic than the control compounds **6** and **13** despite their cellular uptake (Figure 2b). We hypothesize that the greater steric hindrance of the alcohols in **1** and **2** relative to **13** might decrease the ten-

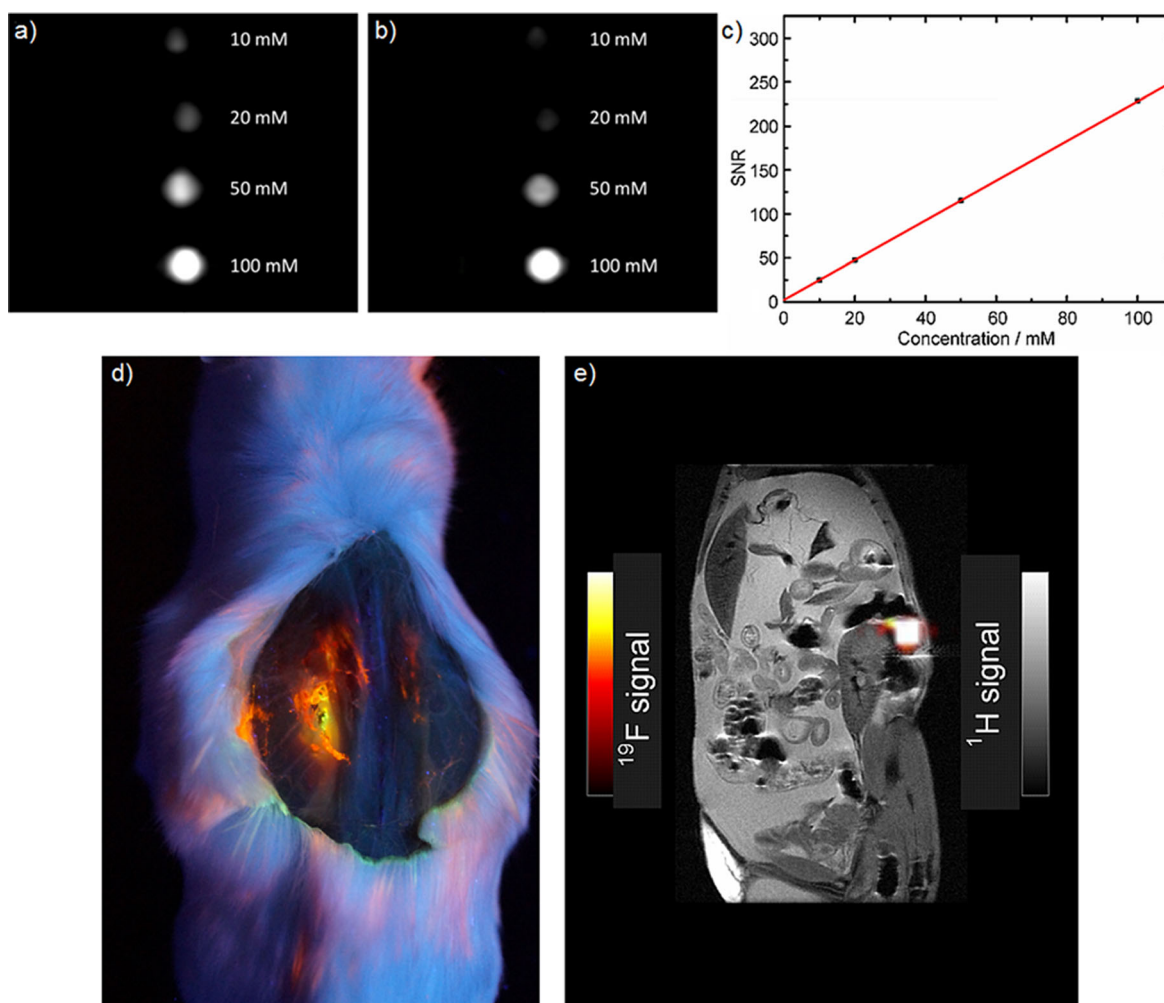


Figure 3.

^{19}F MRI of compound **5** in CH_2Cl_2 at various concentrations ranging from 10 to 100 mM, measured with a) FLASH and b) RARE sequences. c) Signal-to-noise ratio (SNR) vs. concentration of compound **5**. d) Black-light ($\lambda_{\text{exc}} = 365 \text{ nm}$) excited fluorescence photograph of a mouse post-mortem, injected with compound **5** (100 μL of a 100 mM solution in CH_2Cl_2). e) Overlay of ^1H (grayscale) and ^{19}F MRI (color) images of the same mouse in panel d.

Table 3. IC_{50} values for dual imaging agents 1 , 2 , 4 , 5 , 6 , and 13 .			
BODIPY	$\text{IC}_{50} [\mu\text{M}]^{[a]}$		
	HUVEC	HepG2	
1	175	155	
2	n.d.	94	
4	n.d.	n.d.	
5	n.d.	n.d.	
6	n.d.	40	
13	n.d.	57	

[a] See the Supporting Information for concentration–viability curves; n.d.: no significant toxicity was detected < 100 μM .

dependency for their cleavage. The steric effect may also be inferred from comparison with compounds **4** and **5**, which possess even more sterically demanding alcohols. However, decreased bioavailability due to storage in lipid-rich cellular domains must also be considered: Preliminary $\log P$ values of >2.5 and >3 for **4** and **5**, respectively, indicate pronounced hydropho-

bicity, which may withdraw our molecules from metabolism as well. Hence, the BODIPYs **4** and **5** show nearly no toxicity against HepG2 cells. A closer look at the IC_{50} values in HUVEC shows that the carboxylic acid **6** is nontoxic against these cells. This fact indicates that compound **6** is probably not absorbed by HUVEC, whereas HepG2 cells could uptake BODIPY **6** via anion transporters,^[24] which would explain the toxicity of compound **6** therein. Also, compounds **1** and **2** exhibit lower toxicity in HUVEC than in the HepG2 cell line (Figures S5/6 and S12/13). Moreover, the esters **4** and **5** did not show toxicity at any of the concentrations tested (Figures S23/S24 and S30/31), presumably for the same reasons as in HepG2 cells. Taken together, comparison of the MTT assays in HUVEC and HepG2 cells revealed lower toxicity for all compounds in the primary cells. In summary, the dual imaging agents **4** and **5** are promising candidates for in vivo tests given the tolerance by living cells.

Conclusions

To demonstrate the principle that BODIPY dyes and ^{19}F MRI are combinable, five dual FLI/ ^{19}F MRI reporters were synthesized in this study. The fluorescence properties of the fluorescent dyes 1–5 are typical for the BODIPY class with high intensity at low concentrations and narrow emission bands. After verifying the ^{19}F MR activity of all synthesized compounds, the concentration measurements proved that one or two CF_3 groups are insufficient to produce a strong ^{19}F magnetic resonance signal. The detection limit of 8×10^{17} spins is best realized by a large number of chemically and magnetically identical fluorine atoms in the form of CF_3 groups, and may be undercut by another order of magnitude.^[8c] Compounds 4 and 5, with six and nine CF_3 groups, respectively, are decorated enough to produce bright MR signals at low-millimolar concentrations. Improvement of the signal may be obtained by optimizing the image acquisition, which will be described in a forthcoming publication. It should be admitted that practical administration in vivo without local accumulation may hardly produce signals intense enough for ^{19}F MRI due to dilution. We consequently studied the cytotoxicity at lower concentrations, which will be met in whole-body applications. It turned out that the cytotoxicity of the synthesized BODIPYs 1, 2, 4, and 5 depends on the volume of the synthesized esters, which presumably hinders ester hydrolysis. Generally, the cytotoxicity was found to be lower in primary HUVEC, which are closer to the in vivo situation than a cell line. We conclude that the system consisting of BODIPY in conjunction with highly fluorinated alcohols is suitable for dual FLI and ^{19}F MRI by demonstrating that BODIPY 5 can be seen in a mouse post-mortem, both by MRI and FLI. Especially the short relaxation time T_1 and the low toxicity of 4 and 5 makes these compounds valuable starting points for in vivo experiments with water-soluble derivatives. For future biomedical application, we propose 4 as promising candidate, as the remaining protected alcohol function might be exploited for binding the synthesized dual imaging agents covalently to a target of interest, thus decreasing ubiquitous background fluorescence from unbound dye.^[10] In addition, the hydrolytic stability and other pharmacologically relevant parameters must be studied in greater detail before similar compounds can be transferred to live-animal models. Finally, even further expansion to triple contrast agents by combination with ^{18}F PET becomes feasible.^[15]

Experimental Section

General: Reagents and solvents were used as purchased from Sigma–Aldrich, Merck, Acros Organics, and Carbolution Chemicals. The solvents used were dried using common laboratory methods. All air-sensitive reactions were carried out under an argon atmosphere. Analytical thin-layer chromatography (TLC) was performed on Silica Gel 60 on PET-Foils by Fluka Analytik. Column chromatography was performed on a silica gel 60 (63–260 μm).

NMR spectroscopy: ^1H , ^{19}F , and ^{13}C NMR spectra were recorded with a Bruker Avance 2 spectrometer (400, 376 or 100 MHz) at ambient temperature with reference to TMS or solvent standard with

the chemical shifts recorded as δ values in ppm. Multiplicities are denoted as follows: s = singlet, d = doublet, t = triplet, sxt = sextuplet, m = multiplet.

UV/Vis and fluorescence spectroscopy: Absorption spectra were recorded using a commercial spectrophotometer (Jasco, V-650), and fluorescence emission and excitation spectra were obtained with a commercial spectrofluorimeter (Jasco, FP-6500) at micromolar concentrations, if not stated otherwise.

Fluorescence microscopy: For fluorescence microscopy 250 000 cells per well were seeded on glass coverslips in a 24-well format. Cells were incubated with the respective dye at a concentration of 50 μM for 1 h. After washing twice with PBS, cells were fixed for 15 min with 4% PBS-buffered formalin and counterstained with DAPI (2 $\mu\text{g mL}^{-1}$ in PBS) for 10 min. Coverslips were mounted using Fluorsave™ mounting medium (Merck Millipore). Images were obtained and analyzed with an Axio Observer Z1 epifluorescence microscope (Zeiss; DAPI imaging: $\lambda_{\text{exc}} = 335\text{--}383$ nm, $\lambda_{\text{em}} = 420\text{--}470$ nm; FITC imaging: $\lambda_{\text{exc}} = 455\text{--}495$ nm, $\lambda_{\text{em}} = 505\text{--}555$ nm).

MTT assays: MTT [3-(4,5-dimethylthiazol-2-yl)-2,5-diphenyltetrazolium bromide] assays were performed as previously described.^[25] Primary human umbilical vein cells (HUVEC) were isolated from umbilical cords by digestion with 0.01% collagenase A solution (Roche) and grown in ECGM with supplement mix (Promocell) containing penicillin (100 U mL^{-1}), streptomycin (100 $\mu\text{g mL}^{-1}$), kanamycin (50 $\mu\text{g mL}^{-1}$), and 10% FCS (Sigma). Umbilical cords were obtained with the consent of patients (permission by the local ethics committee). For experiments, cells were used at passage 3 or 4.^[22,26] HUVEC or HepG2 cells were seeded at a density of 20 000 or 10 000 cells per well, respectively. Cells were incubated with the tested compounds for 24 h prior to MTT assay. Compounds were dissolved in DMSO and used at the following concentrations: 1, 10, 20, 40, 50, and 100 μM . DMSO served as solvent control. The IC_{50} values were extrapolated from the resulting concentration–viability curves.

Relaxometry: The relaxation times were measured with a benchtop device by Bruker (Minispec mq60, 60 MHz, 1.41 T). The longitudinal relaxation times T_1 were recorded with the inversion recovery sequence, and the transverse relaxation times T_2 with the Car–Purcell–Meiboom–Gill (CPMG) sequence.

^{19}F and ^1H MRI: In vitro and ex vivo magnetic resonance imaging (MRI) was performed with a 9.4 T MRI animal scanner (Biospec Avance III 94/20; Bruker Biospin GmbH, Ettlingen, Germany) with a maximum field strength of 675 mT m^{-1} , linear inductive rise time of 130 μs , and maximum slew rate of 4673 $\text{mT m}^{-1} \text{s}^{-1}$ (BGA12S gradient system; Bruker Biospin GmbH, Ettlingen, Germany), run with ParaVision 5.1 (Bruker Biospin GmbH, Ettlingen, Germany). Measurements were conducted with a linear MRI transceiver tunable both for ^{19}F and ^1H , designed for imaging of rat whole body, with an inner diameter of 72 mm. For both in vitro and ex vivo imaging, ^1H MRI with fast low angle shot (FLASH) sequences was used for orientation of samples in the magnet and for 1st- and 2nd-order shimming, based on previously recorded field maps (ParaVision 5.1, macro MAPSHIM). In the ex vivo experiments, additional ^1H MR images were recorded with a rapid acquisition relaxation enhanced (RARE) sequence, for demonstration of animal morphology and image fusion with ^{19}F MRI data. ^{19}F basic frequency, reference pulse gain, and receiver gain were set manually employing MR spectroscopy pulse programs and TopSpin 2.0PV software (Bruker Biospin GmbH, Ettlingen, Germany). ^{19}F MRI was performed with FLASH

Sequence	Use	FOV [mm] ^[b]	MTX [voxels] ^[c]	TR [ms] ^[d]	TE [ms] ^[e]	NA ^[f]	ST [mm] ^[g]	Duration
^1H RARE	ex vivo	48×32	480×320	1647.3	9.7	8	1	12 min 31 s
^{19}F FLASH	in vitro	64×32	64×32	2000	1.7	32	5	17 min 4 s
	ex vivo	48×32	48×32					
^{19}F RARE	in vitro	64×32	64×32	2400	126.9	128	5	5 min 7 s
	ex vivo	48×32	48×32					

[a] $B_0=9.4\text{ T}$ in CH_2Cl_2 at room temperature; concentration as indicated in Figure 3. [b] Field of view. [c] Matrix size. [d] Repetition time. [e] Echo time. [f] Number of acquisitions. [g] Slice thickness.

and RARE sequences optimized for high signal-to-noise ratio and scan times reasonable for in vivo imaging. Sequence details are summarized in Table 4. For characterization by MRI, compound **5** was dissolved in CH_2Cl_2 at 10, 20, 50, and 100 mm. For each concentration, a volume of 500 μL in a standard plastic reaction vial was placed in the magnet and submitted to MRI as described. Detectability in animals was tested in three mice sacrificed beforehand by CO_2 inhalation, by intramuscular injection of 100 μL of the 100 mm dilution that had been tested before in the in vitro examination, and subsequent MRI.

Syntheses

General procedure A: BODIPY carboxylic acid and DMAP (1.0 equiv) were dissolved in CH_2Cl_2 and cooled to 0°C . After stirring for 10 min, DCC (1.0 equiv) was added and stirred for an additional 1 h. Then the alcohol (1.0 equiv) was added and the reaction mixture was allowed to warm to room temperature. After stirring for 24 h, the obtained suspension was filtered over a small silica gel layer (3 cm). The layer was washed with CH_2Cl_2 , and the filtrate was evaporated under reduced pressure. The received crude product was purified by flash chromatography with silica.

General procedure B: Alcohol, BODIPY **6** (3.0 equiv), DMAP (3.3 equiv), and $\text{Sc}(\text{OTf})_3$ (0.6 equiv) were dissolved in CH_2Cl_2 and stirred for 30 min at -8°C . After adding DIPC (3.2 equiv), the reaction mixture was stirred 30 min at -8°C and an additional 2 d at room temperature. The obtained suspension was filtered over a small silica gel layer (3 cm). After washing the layer with CH_2Cl_2 , the filtrate was washed with HCl (0.1 M, 2 \times), diluted Na_2CO_3 solution (2 \times) and distilled water. The organic phase was then dried over Na_2SO_4 , and the solvent was removed under reduced pressure. The obtained crude product was purified by SiO_2 flash chromatography.

BODIPY 1 was synthesized according to general procedure A. The crude product was purified by column chromatography (silica gel, petroleum ether (PE)/ CH_2Cl_2 2:1, $R_f=0.10$) to give a red solid (0.11 g, 0.27 mmol, yield 91%). ^1H NMR (CDCl_3): $\delta=5.99$ (s, 2H), 4.42 (q, 2H, $^3J_{\text{H,F}}=8.28$ Hz), 2.94 (m, 2H), 2.53 (t, 2H, $^3J_{\text{H,H}}=7.28$ Hz), 2.44 (s, 6H), 2.34 (s, 6H), 1.92 ppm (m, 2H); ^{13}C NMR (CDCl_3): $\delta=170.9$, 154.3, 144.4, 140.3, 131.4, 121.9, 60.6, 33.5, 27.2, 26.4, 16.3, 14.4 ppm; ^{19}F NMR (CDCl_3): $\delta=-70.27$ (s, 3F, CF_3), -146.72 ppm (m, 2F, BF_2); HRMS (ESI): calcd for $\text{C}_{19}\text{H}_{23}\text{BF}_5\text{N}_2\text{O}_2$ [$M+H$] 417.1773, found 417.1768.

BODIPY 2 was synthesized according to general procedure A. The crude product was purified by column chromatography (silica gel PE/ CH_2Cl_2 2:1, $R_f=0.22$) to give a red solid (0.11 g, 0.27 mmol, yield 91%). ^1H NMR (CDCl_3): $\delta=6.00$ (s, 2H), 5.71 (sxt, 1H, $^3J_{\text{H,F}}=6.02$ Hz),

2.96 (m, 2H), 2.63 (t, 2H, $^3J_{\text{H,H}}=7.28$ Hz), 2.45 (s, 6H), 2.34 (s, 6H), 1.94 ppm (m, 2H); ^{13}C NMR (CDCl_3): $\delta=169.5$, 154.5, 143.9, 140.3, 131.4, 122.0, 60.6, 33.1, 27.1, 26.2, 16.3, 14.5 ppm; ^{19}F NMR (CDCl_3): $\delta=-73.25$ (s, 6F, CF_3), -146.58 ppm (m, 2F, BF_2); HRMS (ESI): calcd for $\text{C}_{20}\text{H}_{22}\text{BF}_8\text{N}_2\text{O}_2$ [$M+H$] 484.1647, found 485.1642.

BODIPY 3 was synthesized according to general procedure A. The crude product was purified by column chromatography (silica gel, PE/ CH_2Cl_2 2:1, $R_f=0.19$) to give a red solid (0.13 g, 0.25 mmol, yield 82%). ^1H NMR (CDCl_3): $\delta=5.99$ (s, 2H), 3.01 (m, 2H), 2.78 (t, 2H, $^3J_{\text{H,H}}=7.03$ Hz), 2.44 (s, 6H), 2.35 (s, 6H), 2.00 ppm (m, 2H); ^{13}C NMR (CDCl_3): $\delta=187.6$, 168.6, 154.5, 144.0, 140.3, 134.6, 131.4, 128.2, 121.9, 112.8, 33.1, 27.1, 26.3, 16.3, 14.5 ppm; ^{19}F NMR (CDCl_3): $\delta=-146.58$ (m, 2F, BF_2), -152.71 (m, 2F), -157.57 (t, 1F, $^3J_{\text{F,F}}=21.80$), -162.03 ppm (m, 2F); HRMS (ESI): calcd for $\text{C}_{23}\text{H}_{20}\text{BF}_7\text{N}_2\text{O}_2$ [$M+H$] 501.1584, found 501.1580.

BODIPY 4 was synthesized according to general procedure B. The crude product was purified by column chromatography (silica gel, PE/EtOAc 7:3, $R_f=0.55$) to give a red solid (0.13 g, 0.14 mmol, yield 99%). ^1H NMR (CDCl_3): $\delta=6.07$ (s, 2H), 4.12 (s, 2H), 4.09 (s, 6H), 3.02 (m, 2H), 2.53 (s, 6H), 2.51 (t, 2H, $^3J_{\text{H,H}}=7.28$ Hz), 2.43 (s, 6H), 2.07 (s, 3H), 1.95 ppm (m, 2H); ^{13}C NMR (CDCl_3): $\delta=171.3$, 169.7, 154.0, 144.2, 140.0, 131.1, 121.5, 121.2, 118.3, 65.7, 60.4, 60.2, 43.7, 33.2, 26.0, 20.0, 15.9, 14.1 ppm; ^{19}F NMR (CDCl_3): $\delta=-70.27$ (s, 18F, CF_3), -146.72 ppm (q, 2F, BF_2); HRMS (ESI): calcd for $\text{C}_{32}\text{H}_{30}\text{BF}_{20}\text{N}_2\text{O}_6$ [$M-H$] 929.1878, found 929.1873.

BODIPY 5 was synthesized according to general procedure B. The crude product was purified by column chromatography (silica gel, PE/EtOAc 8:2, $R_f=0.31$ (PE/EE, 9:1)) to give a red solid (0.25 g, 0.23 mmol, yield 82%). ^1H NMR (CDCl_3): $\delta=6.07$ (s, 2H), 4.10 (s, 2H), 4.06 (s, 6H), 3.00 (m, 2H), 2.53 (s, 6H), 2.50 (t, 2H, $^3J_{\text{H,H}}=7.28$ Hz), 2.42 (s, 6H), 1.96 ppm (m, 2H); ^{13}C NMR (CDCl_3): $\delta=171.3$, 154.4, 144.5, 140.3, 121.9, 121.5, 118.6, 64.9, 59.8, 45.3, 33.3, 27.2, 26.3, 16.1, 14.5 ppm; ^{19}F NMR (CDCl_3): $\delta=-70.37$ (s, 27F, CF_3), -146.55 ppm (q, 2F, BF_2); HRMS (ESI): calcd for $\text{C}_{34}\text{H}_{27}\text{BF}_{29}\text{N}_2\text{O}_5$ [$M-H$] 1105.1550, found 1105.1544.

Alcohol 11 was synthesized according to published reaction conditions (yield 57%).^[17] ^1H NMR (CDCl_3): $\delta=7.30$ – 7.19 (m, 5H), 4.44 (s, 2H), 4.13 (s, 2H), 3.62–3.53 (m, 4H), 3.41 (s, 2H), 1.99 ppm (s, 3H); ^{13}C NMR (CDCl_3): $\delta=171.8$, 137.7, 128.5, 127.9, 127.6, 73.7, 71.1, 63.7, 63.2, 44.9, 20.8 ppm; HRMS (ESI): calcd for $\text{C}_{14}\text{H}_{19}\text{O}_5$ [$M-H$] 267.1232, found 267.1227.

Alcohol 12 was synthesized according to published reaction conditions (yield 36% over two steps).^[17] ^1H NMR (CDCl_3): $\delta=4.15$ (s, 2H), 4.09 (s, 4H), 3.59 (s, 2H), 2.10 (s, 3H); ^{13}C NMR (CDCl_3): $\delta=171.1$, 121.6, 118.7, 66.5, 61.1, 59.7, 45.8, 20.4 ppm; ^{19}F NMR (CDCl_3): $\delta=-70.38$ ppm (s).

BODIPY 13 was synthesized according to general procedure A. The crude product was purified by column chromatography (silica gel, PE/EtOAc 8:2, $R_f=0.71$ (PE/EE, 8:2)) to give a red solid (0.10 g, 0.28 mmol, yield 95%). $^1\text{H NMR}$ (CDCl_3): $\delta=5.98$ (s, 2H), 4.09 (q, 2H), 2.92 (m, 2H), 2.44 (s, 6H), 2.41 (t, 2H, $^3J_{\text{H,H}}=7.28$ Hz), 2.35 (s, 6H), 1.87 (m, 2H), 1.21 ppm (t, 3H); $^{13}\text{C NMR}$ (CDCl_3): $\delta=172.6$, 154.2, 145.1, 140.4, 131.5, 121.7, 80.7, 34.4, 29.7, 27.5, 28.8, 16.4 ppm; $^{19}\text{F NMR}$ (CDCl_3): $\delta=-146.58$ ppm (q, BF_2); HRMS (ESI): calcd for $\text{C}_{19}\text{H}_{26}\text{BF}_2\text{N}_2\text{O}_2$ [$M+H$] 363.2055, found 363.2052.

Acknowledgements

Financial support by the German Science Foundation (DFG), JU650/3-1 is gratefully acknowledged. We also thank Dr. Yulin Qi (Saarland University) for recording mass spectra, Theo Ranßweiler for all cell culture work, and Dr. Volker Huch (Saarland University) for recording and analyzing X-ray crystallographic data.

Keywords: fluorescence · imaging agents · radiopharmaceuticals · toxicology

- [1] a) L. Frullano, T. Meade, *J. Biol. Inorg. Chem.* **2007**, *12*, 939–949; b) L. E. Jennings, N. J. Long, *Chem. Commun.* **2009**, 3511–3524; c) M. Srinivas, I. Melero, E. Kaempgen, C. G. Figidor, I. J. M. de Vries, *Contrast Media Mol. Imaging* **2013**, *8*, 432–438.
- [2] a) M. M. Hüber, A. B. Staubli, K. Kustedjo, M. H. B. Gray, J. Shih, S. E. Fraser, R. E. Jacobs, T. J. Meade, *Bioconjugate Chem.* **1998**, *9*, 242–249; b) G. Schneider, R. Seidel, M. Uder, D. Wagner, H.-J. Weinmann, B. Kraumann, *Invest. Radiol.* **2000**, *35*, 564–570; c) M. Modo, D. Cash, K. Mello-dew, S. C. R. Williams, S. E. Fraser, T. J. Meade, J. Price, H. Hodges, *NeuroImage* **2002**, *17*, 803–811; d) M. Modo, K. Mellodew, D. Cash, S. E. Fraser, T. J. Meade, J. Price, S. C. R. Williams, *NeuroImage* **2004**, *21*, 311–317; e) G. Mazooz, T. Mehlman, T.-S. Lai, C. S. Greenberg, M. W. Dewhirst, M. Neeman, *Cancer Res.* **2005**, *65*, 1369–1375.
- [3] a) D. R. Martin, *Am. J. Kidney Dis.* **2010**, *56*, 427–430; b) N. Jalandhara, R. Arora, V. Batuman, *Clin. Pharmacol. Ther.* **2011**, *89*, 920–923; c) P. Stratta, C. Canavese, M. Quaglia, R. Fenoglio, *Rheumatology* **2010**, *49*, 821–823; d) J. Kay, L. Czirják, *Ann. Rheum. Dis.* **2010**, *69*, 1895–1897.
- [4] S. Laurent, D. Forge, M. Port, A. Roch, C. Robic, L. Vander Elst, R. N. Muller, *Chem. Rev.* **2008**, *108*, 2064–2110.
- [5] D. Pan, A. H. Schmieder, S. A. Wickline, G. M. Lanza, *Tetrahedron* **2011**, *67*, 8431–8444.
- [6] a) G. N. Holland, P. A. Bottomley, W. S. Hinshaw, *J. Magn. Reson.* **1977**, *28*, 133–136; b) R. P. Mason, P. P. Antich, E. E. Babcock, J. L. Gerberich, R. L. Nunnally, *Magn. Reson. Imaging* **1989**, *7*, 475–485; c) K. L. Meyer, M. J. Carvlin, B. Mukherji, H. A. Sloviter, P. M. Joseph, *Invest. Radiol.* **1992**, *27*, 620–626; d) A. Kimura, M. Narazaki, Y. Kanazawa, H. Fujiwara, *Magn. Reson. Imaging* **2004**, *22*, 855–860; e) A. M. Morawski, P. M. Winter, X. Yu, R. W. Fuhrhop, M. J. Scott, F. Hockett, J. D. Robertson, P. J. Gaffney, G. M. Lanza, S. A. Wickline, *Magn. Reson. Med.* **2004**, *52*, 1255–1262; f) E. T. Ahrens, R. Flores, H. Xu, P. A. Morel, *Nat. Biotechnol.* **2005**, *23*, 983–987; g) A. M. Neubauer, J. Myerson, S. D. Caruthers, F. D. Hockett, P. M. Winter, J. Chen, P. J. Gaffney, J. D. Robertson, G. M. Lanza, S. A. Wickline, *Magn. Reson. Med.* **2008**, *60*, 1066–1072; h) J. M. Janjic, M. Srinivas, D. K. K. Kadayakkara, E. T. Ahrens, *J. Am. Chem. Soc.* **2008**, *130*, 2832–2841.
- [7] Y. Nosé, *Artif. Organs* **2004**, *28*, 807–812.
- [8] a) Z.-X. Jiang, X. Liu, E.-K. Jeong, Y. B. Yu, *Angew. Chem. Int. Ed.* **2009**, *48*, 4755–4758; *Angew. Chem.* **2009**, *121*, 4849–4852; b) X. Yue, Z. Wang, L. Zhu, Y. Wang, C. Qian, Y. Ma, D. O. Kiesewetter, G. Niu, X. Chen, *Mol. Pharm.* **2014**, *11*, 4208–4217; c) I. Tirotta, A. Mastropietro, C. Cordiglieri, L. Gazzera, F. Baggi, G. Baselli, M. G. Bruzzone, I. Zucca, G. Cavallo, G. Terraneo, F. Baldelli Bombelli, P. Metrangolo, G. Resnati, *J. Am. Chem. Soc.* **2014**, *136*, 8524–8527.
- [9] Q. T. Nguyen, R. Y. Tsien, *Nat. Rev. Cancer* **2013**, *13*, 653–662.
- [10] G. M. van Dam, G. Themelis, L. M. A. Crane, N. J. Harlaar, R. G. Pleijhuis, W. Kelder, A. Sarantopoulos, J. S. de Jong, H. J. G. Arts, A. G. J. van der Zee, J. Bart, P. S. Low, V. Ntziachristos, *Nat. Med.* **2011**, *17*, 1315–1319.
- [11] a) T. Nakamura, F. Sugihara, H. Matsushita, Y. Yoshioka, S. Mizukami, K. Kikuchi, *Chem. Sci.* **2015**, *6*, 1986–1990; b) S. Bo, C. Song, Y. Li, W. Yu, S. Chen, X. Zhou, Z. Yang, X. Zheng, Z.-X. Jiang, *J. Org. Chem.* **2015**, *80*, 6360–6366.
- [12] B. Hinkeldey, A. Schmitt, G. Jung, *ChemPhysChem* **2008**, *9*, 2019–2027.
- [13] a) A. Loudet, K. Burgess, *Chem. Rev.* **2007**, *107*, 4891–4932; b) R. Ziessel, G. Ulrich, A. Harriman, *New J. Chem.* **2007**, *31*, 496–501; c) G. Ulrich, R. Ziessel, A. Harriman, *Angew. Chem. Int. Ed.* **2008**, *47*, 1184–1201; *Angew. Chem.* **2008**, *120*, 1202–1219; d) H. Kobayashi, M. Ogawa, R. Alford, P. L. Choyke, Y. Urano, *Chem. Rev.* **2010**, *110*, 2620–2640; e) S. Suzuki, M. Kozaki, K. Nozaki, K. Okada, *J. Photochem. Photobiol. C* **2011**, *12*, 269–292; f) N. Boens, V. Leen, W. Dehaen, *Chem. Soc. Rev.* **2012**, *41*, 1130–1172.
- [14] a) I. D. Johnson, H. C. Kang, R. P. Haugland, *Anal. Biochem.* **1991**, *198*, 228–237; b) J. Karolin, L. B. A. Johansson, L. Strandberg, T. Ny, *J. Am. Chem. Soc.* **1994**, *116*, 7801–7806; c) H. L. Kee, C. Kirmaier, L. Yu, P. Thamyongkit, W. J. Youngblood, M. E. Calder, L. Ramos, B. C. Noll, D. F. Bocian, W. R. Scheidt, R. R. Birge, J. S. Lindsey, D. Holtz, *J. Phys. Chem. B* **2005**, *109*, 20433–20443.
- [15] a) Z. Li, T.-P. Lin, S. Liu, C.-W. Huang, T. W. Hudnall, F. P. Gabbai, P. S. Conti, *Chem. Commun.* **2011**, 47, 9324–9326; b) J. A. Hendricks, E. J. Keliher, D. Wan, S. A. Hilderbrand, R. Weissleder, R. Mazitschek, *Angew. Chem. Int. Ed.* **2012**, *51*, 4603–4606; *Angew. Chem.* **2012**, *124*, 4681–4684; c) S. Liu, T.-P. Lin, L. Leamer, H. Shan, Z. Li, F. P. Gabbai, P. S. Conti, *Theranostics* **2013**, *3*, 181–189; d) E. J. Keliher, J. A. Klubnick, T. Reiner, R. Mazitschek, R. Weissleder, *ChemMedChem* **2014**, *9*, 1368–1375.
- [16] a) Z. Li, E. Mintzer, R. Bittman, *J. Org. Chem.* **2006**, *71*, 1718–1721; b) D. Wang, J. Fan, X. Gao, B. Wang, S. Sun, X. Peng, *J. Org. Chem.* **2009**, *74*, 7675–7683.
- [17] Z.-X. Jiang, Y. B. Yu, *Tetrahedron* **2007**, *63*, 3982–3988.
- [18] H. Zhao, A. Pendri, R. B. Greenwald, *J. Org. Chem.* **1998**, *63*, 7559–7562.
- [19] M. Bouchra, P. Calinaud, J. Gelas, *Synthesis* **1995**, 561–565.
- [20] M. Shah, K. Thangaraj, M.-L. Soong, L. T. Wolford, J. H. Boyer, I. R. Politzer, T. G. Pavlopoulos, *Heteroat. Chem.* **1990**, *1*, 389–399.
- [21] C. Spies, A.-M. Huynh, V. Huch, G. Jung, *J. Phys. Chem. C* **2013**, *117*, 18163–18169.
- [22] K. Astanina, Y. Simon, C. Cavalius, S. Petry, A. Kraegeloh, A. K. Kiemer, *Acta Biomater.* **2014**, *10*, 4896–4911.
- [23] a) M. S. Tsuboy, J. P. F. Angeli, M. S. Mantovani, S. Knasmüller, G. A. Umbuzeiro, L. R. Ribeiro, *Toxicol. In Vitro* **2007**, *21*, 1650–1655; b) M. I. Thabrew, R. D. Hughes, I. G. McFarlane, *J. Pharm. Pharmacol.* **1997**, *49*, 1132–1135; c) C.-L. Huang, C.-C. Huang, F.-D. Mai, C.-L. Yen, S.-H. Tzing, H.-T. Hsieh, Y.-C. Ling, J.-Y. Chang, *J. Mater. Chem. B* **2015**, *3*, 651–664.
- [24] a) K. Koike, T. Kawabe, T. Tanaka, S. Toh, T. Uchiumi, M. Wada, S.-i. Akiyama, M. Ono, M. Kuwano, *Cancer Res.* **1997**, *57*, 5475–5479; b) R. Kikuchi, H. Kusahara, N. Hattori, K. Shiota, I. Kim, F. J. Gonzalez, Y. Sugiyama, *Mol. Pharmacol.* **2006**, *70*, 887–896.
- [25] S. M. Kessler, J. Pokorny, V. Zimmer, S. Laggai, F. Lammert, R. M. Bohle, A. K. Kiemer, *Am. J. Physiol. Gastrointest. Liver Physiol.* **2013**, *304*, G328–G336.
- [26] K. Astanina, M. Koch, C. Jüngst, A. Zumbusch, A. K. Kiemer, *Sci. Rep.* **2015**, *5*, 11453.

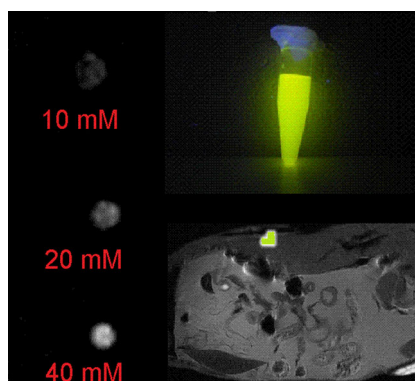
Received: February 28, 2016

Revised: May 25, 2016

Published online on ■■■■■ 0000

FULL PAPERS

Light and magnetism: The combination of fluorescence and ^{19}F MRI is exemplified in a mouse post-mortem by a BODIPY dye highly decorated with fluorine atoms. Up to nine CF_3 groups providing 27 equivalent fluorine atoms are introduced by efficient condensation reactions. A detection limit below 10 μM in ^{19}F MRI together with low toxicity makes the presented compounds a worthy starting point for further development. Local accumulation in vivo will be accomplished by targeting.



A. M. Huynh, A. Müller, S. M. Kessler, S. Henrikus, C. Hoffmann, A. K. Kiemer, A. Bücker, G. Jung*



Small BODIPY Probes for Combined Dual ^{19}F MRI and Fluorescence Imaging

